

Estimation of TOA radiative fluxes from the GERB instrument data

N. Clerbaux, C. Bertrand, S. Dewitte, L. Gonzalez, A. Ipe, B. Nicula

Royal Meteorological Institute of Belgium, Avenue Circulaire 3, B-1180 Brussels, Belgium.

ABSTRACT

The first Meteosat Second Generation (MSG) satellite was launched in August 2002. This EUMETSAT satellite carries 2 new instruments on the geostationary orbit: the Spinning Enhanced Visible and InfraRed Imager, SEVIRI, and the Geostationary Earth Radiation Budget, GERB. The unique feature of GERB in comparison with previous measurement missions of the Earth's radiation budget (e.g. ERBE, ScaRaB and CERES experiments) is the high temporal sampling afforded by the geostationary orbit, albeit for a limited region of the globe. The GERB instrument provides accurate broadband measurements of the radiant energy originating in the reflection of the incoming solar energy by the Earth-atmosphere system and in the thermal emission within this system. The synergetic use of the SEVIRI data is needed to convert these directional measurements (radiances) into radiative fluxes at the top-of-atmosphere. Additionally, the SEVIRI data allows the enhancement of the spatial resolution of the GERB measurement. This paper describes the near real-time GERB processing system that has been set up at the Royal Meteorological Institute of Belgium (RMIB). This includes the unfiltering of the instrument data, the radiance-to-flux conversions and the enhancement of the instrument spatial resolution. An early validation of the instrument data by comparison with CERES data is presented. Finally, the different data formats, the way to access them and their expected accuracy are presented.

Keywords: Earth radiation budget, radiative fluxes, remote sensing

1. INTRODUCTION

On August 28th 2002 the first Geostationary Earth Radiation Budget instrument¹ (GERB-2) was launched on MSG-1, first of the EUMETSAT Meteosat Second Generation series of geostationary satellites.² With this instrument, time continuous broadband measurements of the Earth became available for the first time, thanks to the geostationary orbit. In this sense, this data will complement in a unique way those of broadband instruments on low orbit satellites like ERBE,³ ScaRaB⁴ or CERES.⁵

The GERB data is processed in near real time in the GERB ground segment at the Rutherford Appleton Laboratory (RAL) and at the Royal Meteorological Institute of Belgium (RMIB). RAL is responsible for the generation of Level-1.5 data which mainly consists in the calibration and the geolocation of the raw instrument data, while RMIB is responsible for the determination of unfiltered radiances and fluxes at the Top Of the Atmosphere (TOA) which are the Level-2.0 data.

This paper gives a general overview of the GERB data processing with emphasis on the RMIB part of the processing. Section 2 presents the main characteristics of the GERB instrument and the calibration and geolocation of the data. As most of the GERB data processing relies on narrow band data from the Spinning Enhanced Visible and InfraRed Imager,² this new meteorological imager shortly presented in Sect. 3. The sections 4 to 7 present the estimation of the synthetic long wave radiance, the unfiltering process, the radiance-to-flux conversion and the enhancement of the instrument spatial resolution, respectively. Then, the Level-2 product formats are presented (Sect. 8), with their associated estimated error (Sect. 9). First comparison with CERES-Terra instrument data are presented in Sect. 10.

Send correspondence to Nicolas Clerbaux: E-mail: nicolas.clerbaux@oma.be, Telephone: +32 2 373 0610

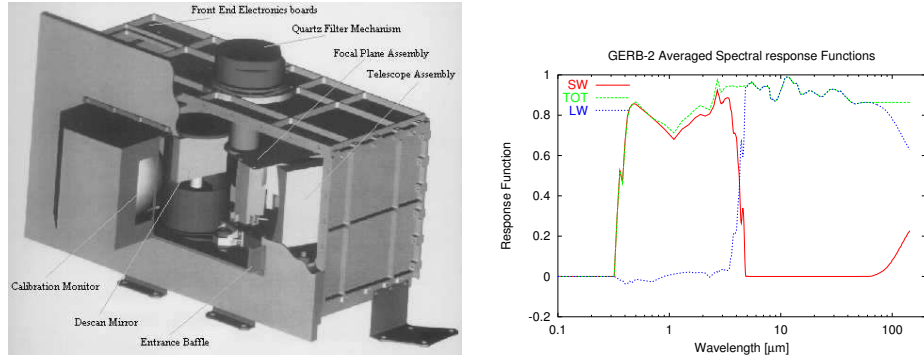


Figure 1. GERB instrument drawing (left) and *Ad-interim* averaged spectral response functions for the GERB-2 instrument (right).

2. GERB INSTRUMENTS

The GERB instrument (Fig. (1)) is a small (45x20x15cm) and accurate broadband radiometer designed for the MSG satellite. As the instrument is located at the edge of this spin-stabilized satellite (100 rpm), it is subjected to strong acceleration (18g) which complicated its mechanical design. In the instrument, the De-Scan Mirror (DSM) has its rotation axis aligned with that of the satellite and rotates in the opposite direction at half the angular velocity of the satellite. This mirror reflects the radiation towards a linear array of 256 detectors that observe a stationary image of Earth for a sustained period of time (about 40ms). At each rotation of the satellite (i.e. each 0.6s) the detectors measure along one North-South swath of the Earth which can be programmed to move in the East-West direction. Using this functionality, a full disk image of the Earth at a spatial resolution of approximately 50 km² is acquired after 282 satellite rotations (or about 2.5 minutes).

The GERB instrument measures broadband radiances with an accuracy better than 1%. The instrument performs successive scans of the Earth disk for total radiation (from about 0.32 to more than 100μm) and, using a quartz filter, for short wave radiation (about $\lambda < 4\mu\text{m}$). The long wave radiation can then be obtained by subtracting the short wave from the total one. The averaged spectral response functions (or spectral sensitivity) for the total, short wave and long wave channels of the GERB-2 instrument are given in Fig. (1). Of course, each detector has its own spectral sensitivity but the differences are very small.

The calibration is known to be of prime importance for Earth radiation studies. Pre-flight ground calibrations of the GERB-1,-2 and -3 instruments have been carried out at Imperial College (London). Those calibrations try to characterize: the instrument's gains in the two channels, the detectors' Point Spread Functions (PSFs), the on-board calibration devices (black body and solar integrating sphere), and the spectral response of the instrument with and without the quartz filter. Concerning the latter, the ground characterization of the spectral response functions for GERB-2 is currently ad-interim because there are plans to reprocess this data in the future.

In addition to pre-flight characterization, on-board monitoring of the calibration over the lifetime in orbit is made possible by a black body source and a solar diffuser. A deep space look is used for zero reference. Measurements of the on-board blackbody are made during every rotation of the satellite, i.e. for each measurement, to ensure that the accuracy requirements are met. The solar diffuser is deployed on a regular basis to determine changes in the short wave measurements due to drift or degradation of the optics.

The geolocation of the GERB data is computed at the RAL based on the position of the instrument De-Scan Mirror provided by an angular positioning sensor and on information about the satellite position and attitude provided by EUMETSAT. The accuracy of the geolocation can be checked, monitored and possibly improved by matching the large GERB footprint in the finer SEVIRI instrument images.

3. SEVIRI SYNERGY

The SEVIRI instrument² generates multi-spectral imagery of the Earth surface and cloud systems every 15 minutes with a spatial resolution of $3km$ at the sub-satellite point ($1km$ for the High Resolution Visible channel). Compared with previous Meteosat satellites, the main improvement is relies on the number of spectral channels which is twelve compared to three for Meteosat. The instrument measures in narrow-band solar channels at $0.6\mu m$, $0.8\mu m$ and $1.6\mu m$, one broadband visible channel (from $0.5\mu m$ to $0.9\mu m$) and eight thermal channels ranging from $3.9\mu m$ to $13.4\mu m$.

As described in the following, SEVIRI narrow band instrument data is used during most of the real time GERB data processing as well as for monitoring and validation activities. As a meteorological satellite imager, the instrument is well-suited for the cloud cover characterization which is of prime importance to describe the radiation field anisotropy at the TOA needed for an accurate conversion of the radiances in fluxes.

The SEVIRI narrow band radiances are also used to estimate the broad band radiances through a standard narrow band to broad band conversion. In this case, the broad band short wave or long wave quantity is estimated using polynomial regression on the imager radiances where the regression coefficients are dependent on the viewing and solar geometry. Obviously, compared with actual GERB measurements, those estimates suffer from the less accurate calibration of the SEVIRI channels (especially for the shortwave) and from inaccuracies introduced by the spectral modeling. However, they allow the generation of GERB products at the improved spatial resolution of 10 km (Sect. 7).

4. GERB LW ESTIMATION

This first step of the processing performs the estimation of a synthetic long wave radiance by subtraction of the shortwave from the total radiance:

$$L_{LW} = L_{TOT} - A L_{SW} \quad (1)$$

The factor A is defined such that L_{LW} is zero when a black body of $5800K$ (solar spectrum) is observed. As there are small differences in the spectral responses, each detector has its own A factor. The spectral response function for the long wave channel in Fig. (1) is defined from the total and short wave spectral responses in an equation similar to Eq. (1). The estimation of the synthetic long wave using Eq. (1) involves a preliminary spatial and temporal interpolation of the measurements. In practice, the total measurements are linearly interpolated at the short wave time and geolocation. In the worst case, the difference in time between their acquisitions is 2.5 minutes. Due to the interpolations, the estimated synthetic long wave may appear noisy in case of fast cloud motion or in case of non-repeatability of the instrument line-of-sight (LOS). The latter case corresponds to a spatial dispersion of the actual measurement off the nominal position. Fig. (2) shows that this dispersion is about one GERB pixel in the East-West direction. The figure illustrates the noise in the GERB synthetic long wave radiance due to the non-repeatability of the LOS: in the left part of the disk (day time) noise is introduced by the subtraction of Eq. 1, while in the right part the long wave is not affected because the SW is zero (night time).

In a second step, the noise affecting the long wave radiance is filtered using an estimate of this broadband radiance by the SEVIRI narrowband radiances (narrowband-to-broadband conversion). The difference between the GERB synthetic long wave radiance and the SEVIRI estimate is limited to 3%.

5. GERB RADIANCES UNFILTERING

The GERB unfiltering is designed for the averaged short wave and long wave spectral response functions for its 256 detectors. The small differences in spectral response function can be corrected before the unfiltering as described in Ref. 6. Because at this time there is no significant difference in spectral response, the processing does not perform this correction. Nevertheless, this correction may be used for future GERB instruments if one or several detectors display non-nominal spectral responses.

For natural scenes, there are small contributions of the emitted thermal radiation to the short wave radiance L_{SW} and of the reflected solar radiance to the synthetic long wave radiance L_{LW} . The former is relatively

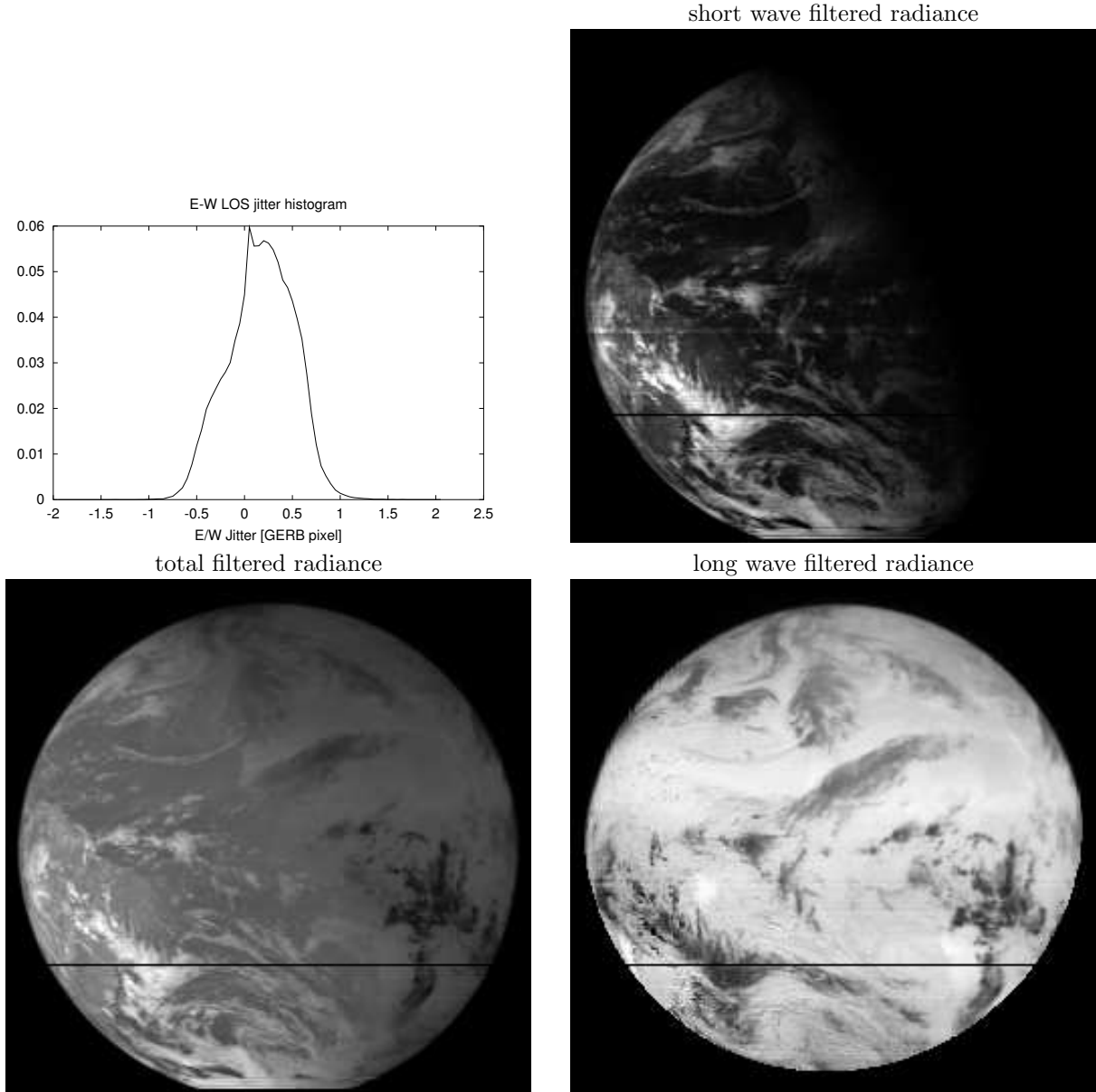


Figure 2. East-West jitter histogram for one GERB image and example of shortwave, total wave and long wave images.

small and can be modeled as a function of the long wave thermal radiance as illustrated by Fig. (3, top-left). On this figure the symbols '+' correspond to radiative transfer computations for 4320 conditions for the Earth-atmosphere system. A detailed description of this data base is given in⁷).

The estimation of the solar contamination in the long wave channel is harder as shown in Fig. (3, top-right). For solar radiation, the residual error of a simple fit:

$$L_{LW} = -1.614 L_{SW} \quad (2)$$

can reach up to $1Wm^{-2}sr^{-1}$ for scenes having a spectral signature very different of the solar spectrum (e.g. ocean). The RMS error on the data base is $0.34Wm^{-2}sr^{-1}$. The estimation of this contamination is improved using spectral information from SEVIRI.

Once the contaminations are subtracted from the measurements, the unfiltered radiances are estimated from the filtered ones as:

$$\begin{aligned} L_{LW}^{uf} &= \alpha_{LW} L_{LW} \\ L_{SW}^{uf} &= \alpha_{SW} L_{SW} \end{aligned} \quad (3)$$

where L_{LW}^{uf} is the unfiltered radiance due to the thermal emission and L_{SW}^{uf} is the one due to the reflection of solar radiation. Bottom plots of Fig. (3) show the unfiltering factors α_{SW} and α_{LW} according to the filtered radiances for the data base mentioned above. Using the polynomial fits displayed in the plots, the RMS error introduced during the unfiltering is about 0.1% for the LW and 0.4% for the SW. This procedure is similar to the one adopted by CERES and described in Ref. 8.

For the GERB unfiltering some spectral information can be extracted from the SEVIRI data and be used to improve the estimation of the contaminations and the unfiltering factors. For example, when the long wave contamination by the solar radiation is estimated using the SEVIRI solar measurements $L_{0.6\mu m}$, $L_{0.8\mu m}$ and $L_{1.6\mu m}$ as:

$$L_{LW} = -0.21 - 0.104L_{0.6\mu m} - 0.027L_{0.8\mu m} + 0.0997L_{1.6\mu m} \quad (4)$$

the RMS error reduces to $0.12Wm^{-2}sr^{-1}$, three times more accurate than the use of Eq. (2). The unfiltering factors are estimated as the ratio of the unfiltered and filtered broadband quantities derived by standard narrowband-to-broadband conversions applied on SEVIRI data:

$$\begin{aligned} \alpha_{LW} &= \frac{L_{LW}^{uf}}{L_{LW}^f} \\ \alpha_{SW} &= \frac{L_{SW}^{uf}}{L_{SW}^f} \end{aligned} \quad (5)$$

On the above data base, the RMS unfiltering error with Eq. (5) is 0.25% for the short wave and 0.025% for the long wave. According to the approach that does not use SEVIRI data, the Eq. (5) allows to improve the unfiltering by reducing the unfiltering error of a factor 2 for the short wave and 4 for the long wave. The better improvement observed for the long wave radtaion is explained by the greater number of SEVIRI channels in the thermal part of the spectrum.

6. GERB ANGULAR MODELING

At this step, the fluxes are estimated from the unfiltered radiances. This requires the use of a model, R , accounting for the angular distribution of the radiance field at the TOA:

$$\begin{aligned} F_{LW} &= \frac{\pi L_{LW}^{uf}}{R(\theta_v)} \\ F_{SW} &= \frac{\pi L_{SW}^{uf}}{R(\theta_s, \theta_v, \phi)} \end{aligned} \quad (6)$$

where θ_s and θ_v are the solar and viewing zenith angles and ϕ is the relative azimuth angle.

For the short wave radiation, the best available models are a set of 590 models $R(\theta_s, \theta_v, \phi_r)$ derived by the CERES inversion team from 8 months of data from the CERES instrument on the Tropical Rainfall Measuring Mission (TRMM) satellite as described in Ref. 9. Each of those models is valid for a given range of surface and cloud cover conditions. A set of ADMs is only valid for a given footprint size. For CERES-TRMM the footprint size at the subsatellite point is 10x10 km which prohibits their direct use for the GERB footprint. For this reason, the ADMs are applied on the SEVIRI estimate of the broadband unfiltered radiances (L_{SW}^{uf} and L_{LW}^{uf} in the Eq. 3) over boxes of 3x3 SEVIRI pixels.

The selection of the best-suited ADM for Eq. (6) needs a characterization of the footprint in terms of surface type, cloud fraction, cloud optical depth and thermodynamical cloud phase. For clear ocean footprints, the

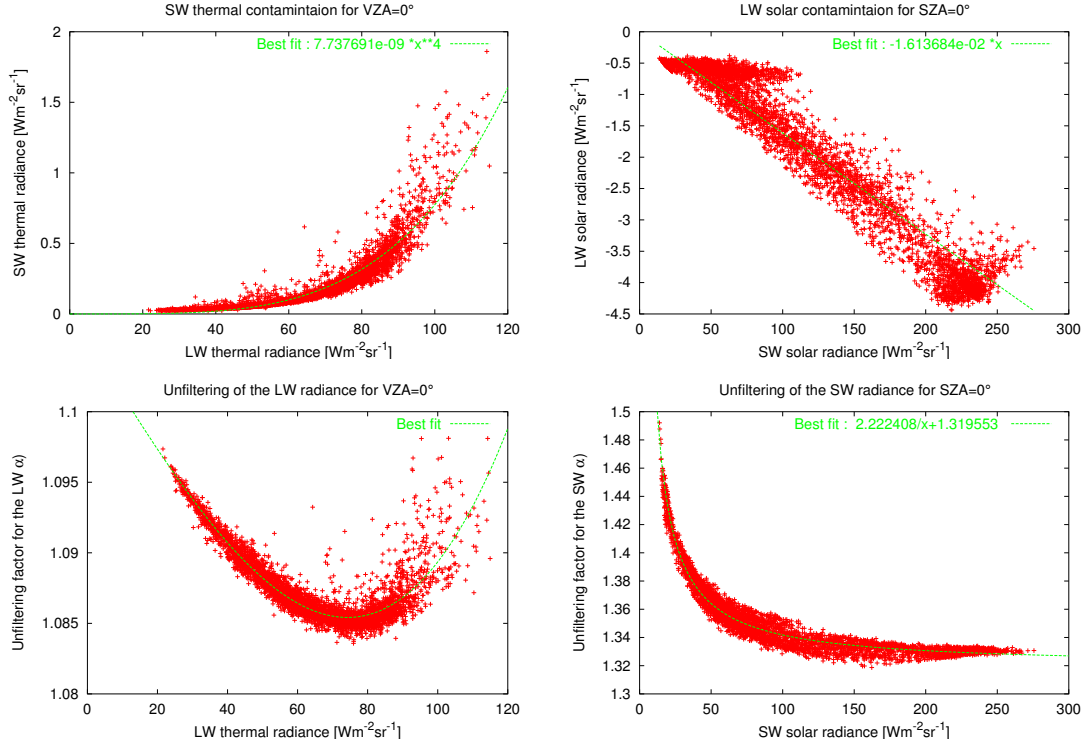


Figure 3. Top: scatter plots of short wave versus long wave radiance for emitted thermal radiation (left) and long wave versus short wave for reflected solar radiation (right). Bottom: scatter plots of unfiltering factor α for the long wave channel (left) and for the short wave channel (right).

angular modeling can be improved using information about surface wind speed and aerosol optical thickness.⁹ Because this information is not yet operationally available over the MSG disk, standard values are used in the GERB data processing. The footprint is characterized as belonging to one of the following surface classes: ocean, moderate-to-high vegetation, low-to-moderate vegetation, dark desert, bright desert or snow. For this, a global IGBP classification¹⁰ at 1km resolution is used. The resulting 6-classes map at the 10km resolution is shown on Fig. (4, a). Once available, fresh snow map derived for the MSG disk will be used. The cloud cover is estimated by comparison of the visible band reflectance at $0.6\mu\text{m}$ and $0.8\mu\text{m}$ with the corresponding reflectance in clear-sky condition. The cloud optical thickness τ is then estimated for each imager pixels using look-up-tables (LUT):

$$\tau = \tau(\rho, \rho_{cs}, \theta_v, \theta_s, \phi); \quad (7)$$

Those LUT were computed using STREAMER radiative transfer model for the 6 CERES surface types and water and ice clouds. The cloud identification takes advantage of the accurate estimation of the clear sky reflectance ρ_{cs} which is made possible by the geostationary orbit as described in Ref. 11. Illustration of the clear sky reflectance image is given on Fig. (4, c). In a second step, a cloud mask is built by thresholding the cloud optical depth. The cloud fraction is then derived for 3×3 pixel boxes (i.e. 10 km resolution). Finally, the averaged cloud optical depth and thermodynamic phase is recomputed for the cloudy part of the boxes. As the above cloud identification relies on the SEVIRI visible channels, it can not be used during night time. This is not a problem because in this case there is no need for ADM selection as there is no solar reflected radiation in Eq. (6).

For the long wave, the CERES-TRMM ADMs are not used because night time cloud identification is outside the scope of the GERB project. We plan to use cloud identification from the EUMETSAT Now Casting Satellite Application Facility, once available. In the meanwhile, a modeling of the limb darkening has been implemented

based on the thermal measurements of SEVIRI, as described in Ref. 7:

$$R(\theta_v) = R(\theta_v, L_{3.9\mu m}, L_{6.2\mu m}, L_{7.3\mu m}, L_{8.7\mu m}, L_{9.7\mu m}, L_{10.8\mu m}, L_{12\mu m}, L_{13.4\mu m}) \quad (8)$$

This approach is similar to the implementation¹² of Schmetz and Liu for Meteosat. As the parameterization of Eq. (8) has been done using plane-parallel radiative transfer computations, the approach leads to an underestimation of the anisotropy over broken cloud fields. As the CERES–TRMM models, this model does not depend on the azimuthal angle of observation. Nevertheless, it has been proved that the azimuthal anisotropy over dry and mountainous regions may lead to a significant overestimation of the flux from the geostationary orbit¹³). Indeed, GERB is always observing the southern faces of the mountains in the northern hemisphere and the northern faces in the southern hemisphere. Currently, those limitations are not compensated for.

7. ENHANCEMENT OF GERB SPATIAL RESOLUTION

Each GERB short wave and long wave radiance is compared with the estimated value from SEVIRI. For this the imager estimate, at the 10 km resolution, is convoluted with the GERB footprint using the detector PSF. The ratio between the actual measurement and the SEVIRI estimation can be used to correct the SEVIRI derived radiances and fluxes provided it is possible to increase the spatial resolution of the ratio from the GERB 50 km resolution to the 10 km spatial resolution.

For this, an iterative processing¹⁴ has been implemented that searches the best correction ratio at the 10 km resolution in such a way that, after correction, the estimated products at the fine spatial resolution are consistent with the GERB measurements.

This can be seen as a kind of correction of the SEVIRI estimated radiances and fluxes for the imager narrow band channel calibration errors and, at least at large spatial scale, for the error introduced by the SEVIRI narrow band to broad band conversion.

8. PRODUCTS CUSTOMIZATION AND DISSEMINATION

The RMIB Level-2 products exist in 3 categories of space and time sampling:

- the Averaged Rectified Geolocated (ARG) products are obtained by averaging three consecutive GERB measurements. The products are rectified on a fixed geolocation grid having the same spatial resolution than the original GERB measurements (the geostationary satellite grid is used). In the ARG product, the spatial shape of one pixel is an average of the different GERB footprints that have contributed to it in the rectification and time averaging process.
- the Snap-shot High-resolution Images (SHI) are snapshot at the SEVIRI acquisition time and for 3*3 SEVIRI pixels. The product is the SEVIRI estimate which have been corrected by GERB through the resolution enhancement process and is directly compatible with others SEVIRI products like cloud identification.
- the Binned Averaged Rectified Geolocated (BARG) are defined as averages over exact 15 minutes bins (first bin is 00:00-00:15UTC, etc). The spatial resolution of this product is about 50 km and is obtained by simple averaging over 5x5 SHI pixels (and then 15x15 SEVIRI pixels). This product aims to simplify the comparison with NWP outputs.

For these 3 categories of products, separate files are generated for short wave and long wave radiation, each containing radiance and flux data as well as some additional information.¹⁵ The SHI product is disseminated for a window over Europe but is available on request over the full disk area.

The GERB data is made available to the user community through 2 different FTP servers: the RAL (<http://ggspspro.ag.rl.ac.uk>) provides access to the climatological archive of ARG products and the RMIB On Line Short-term Service (ROLSS) (<http://gerb.oma.be>) gives access to the three categories of products in *near real time* (meaning within 4 hours).

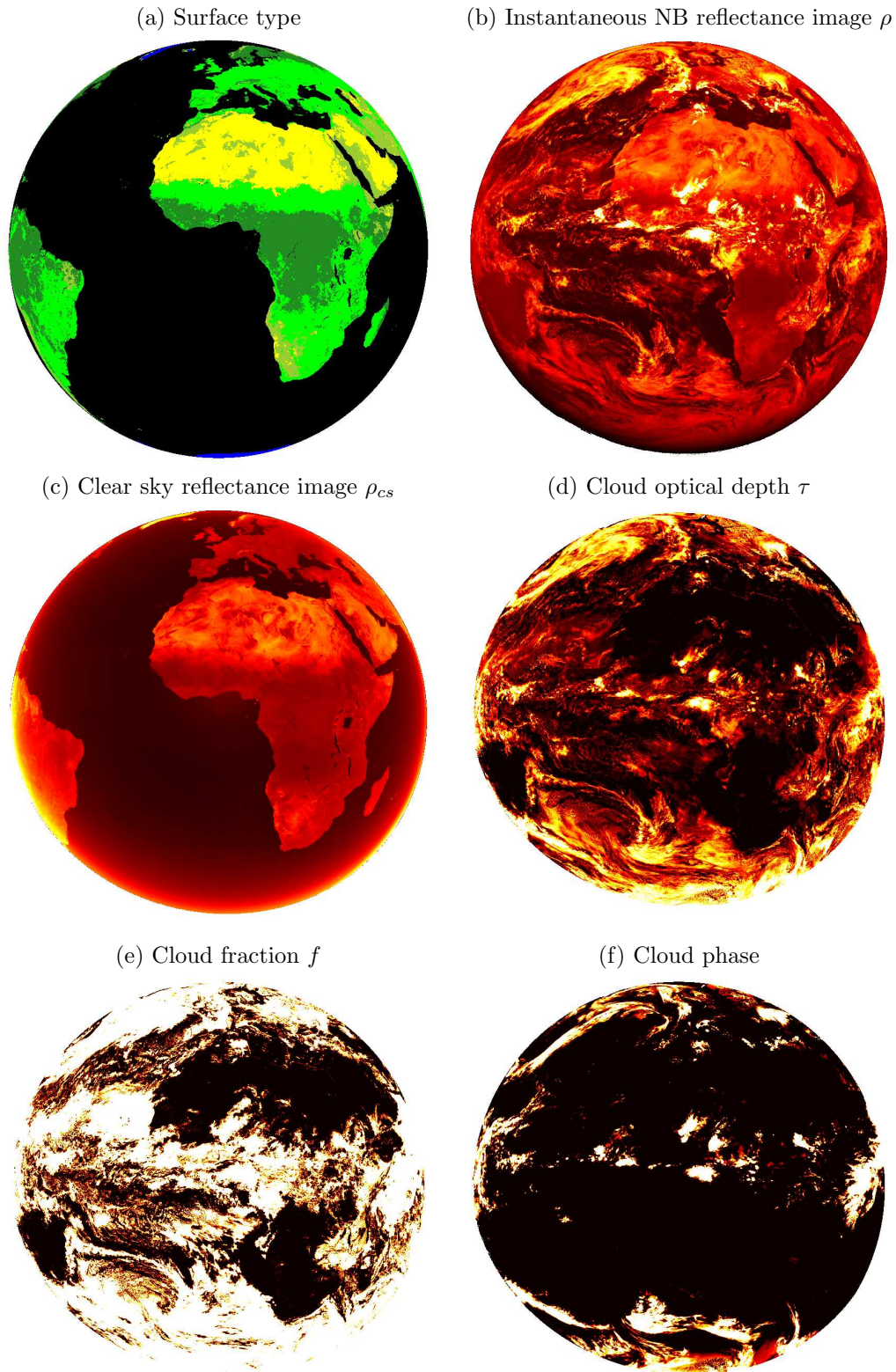


Figure 4. Main results of the GERB/SEVIRI scene identification applied on Meteosat-7 data for 12h, 17th June 2003.

9. ERROR SOURCES AND EXPECTED ACCURACY

Multiple error sources contribute to the errors on the final products. The error sources that are inherent to process of flux estimation from a broadband radiometer are:

- calibration of filtered radiances
- thermal/solar radiance separation
- spectral unfiltering
- radiance to flux conversion

The resulting errors on the unfiltered radiances are summarized in Tab. (1), those on the fluxes are summarized in Tab. (2). The viewing zenith angle of 50 degrees in Tab. (2)-which is the optimum observation angle in terms of flux errors- is representative for the METEOSAT view of Europe.

	thermal radiance	solar radiance
error on absolute scale	0.46%	1.75%
noise level (1 sigma)	$0.22Wm^{-2}sr^{-1}$	$0.30Wm^{-2}sr^{-1}$

Table 1. Summary of errors on the unfiltered radiances due to calibration of filtered radiances, thermal/solar radiance separation and spectral unfiltering.

NADIR VIEW	thermal flux	solar flux
error on absolute scale	8.3%	10.7%
noise level (1 sigma)	$6.2Wm^{-2}$	$10Wm^{-2}$

50 ° VIEW	thermal flux	solar flux
error on absolute scale	1.7%	6.2%
noise level (1 sigma)	$1.2Wm^{-2}$	$5.1Wm^{-2}$

Table 2. Summary of errors on the nadir view (top) and the 50 view (bottom) fluxes due to calibration of filtered radiances, thermal/solar radiance separation, spectral unfiltering and radiance to flux conversion.

10. VALIDATION ACTIVITIES

The validation of the GERB products is an on-going activity. Fig. (5) shows early comparison of GERB and CERES-Terra colocated and coangular unfiltered short wave and long wave radiances. For this kind of comparison, one CERES instrument is operated in a particular scanning mode that maximizes the number of coangular measurement. The scatter plots indicate a 1% and 2% difference for the shortwave and long wave measurement, respectively:

$$\begin{aligned} \frac{GERB_{SW}}{CERES_{SW}} &= 1.011 \pm 0.013 \\ \frac{GERB_{LW}}{CERES_{LW}} &= 0.980 \pm 0.034 \end{aligned} \quad (9)$$

Of course, the radiance level validations will continue and will be followed by flux level data validation.

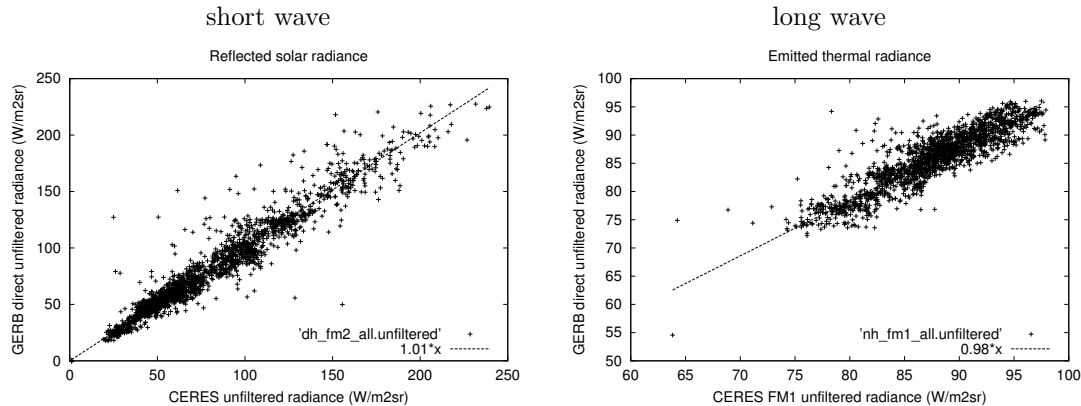


Figure 5. Early validation of GERB unfiltered radiance: scatter plots of coangular and colocated GERB and CERES-Terra data.

11. CONCLUSIONS

The conversion of GERB filtered geolocated radiances (Level-1.5 data) in unfiltered radiances and fluxes data (Level-2) is described in this paper. For this processing, state of the art accuracy is obtained thanks to the synergetic use of the 12 SEVIRI channels and the use of the set of ADMs derived from CERES-TRMM.

ACKNOWLEDGMENTS

The development of the GERB processing described in this paper was supported by the Belgian Office of Science, technical and Cultural (OSTC) matter through the PRODEX program and by the European Commission through the 4th framework program.

REFERENCES

1. J. E. Harries and D. Crommelynck, “The geostationary earth radiation budget experiment on MSG-1 and its potential applications,” *Advances in Space Research* **24**, pp. 915–919, 1999.
2. J. Schmetz, P. Pili, S. Tjemkes, D. Just, J. Kerkmann, S. Rota, and A. Ratier, “An introduction to meteosat second generation (msg),” *Bulletin of the American Meteorological Society* **83**, pp. 977–992, 2002.
3. B. R. Barkstrom, “The earth radiation budget experiment (ERBE),” *Bulletin of the American Meteorological Society* **65**, pp. 1170–1186, 1984.
4. R. Kandel, M. Viollier, P. Raberanto, J. P. Duvel, L. A. Pakhomov, V. A. Golovko, A. P. Trishchenko, J. Mueller, E. Raschke, R. Stuhlmann, and the ISSWG, “The ScaRaB earth radiation budget dataset,” *Bulletin of the American Meteorological Society* **79**, pp. 765–783, 1998.
5. B. A. Wielicki, B. R. Barkstrom, E. F. Harrison, R. B. Lee III, G. L. Smith, and J. E. Cooper, “Clouds and the earth’s radiant energy system (CERES): An earth observing system experiment,” *Bulletin of the American Meteorological Society* **77**, pp. 853–868, 1996.
6. N. Clerbaux, “Correction of the dispersion in the gerb’s detector spectral response curves,” Technical Note MSG-RMIB-GE-TN-0031, RMIB, December 1999.
7. N. Clerbaux, S. Dewitte, L. Gonzalez, C. Bertand, B. Nicula, and A. Ipe, “Outgoing longwave flux estimation: Improvement of angular modelling using spectral information,” *Remote Sensing of Environment* **85**, pp. 389–395, 2003.
8. N. Loeb, K. Priestley, D. Kratz, E. Geier, R. Green, B. Wielicki, P. Hinton, and S. Nolan, “Determination of unfiltered radiances from the clouds and the earth’s radiant energy system instrument,” *Journal of Applied Meteorology* **40**, pp. 822–835, 2001.

9. N. Loeb, N. Smith, S. Kato, W. Miller, S. Gupta, P. Minnis, and B. Wielicki, "Angular distribution models for top-of-atmosphere radiative flux estimation from the clouds and the earth's radiant energy system instrument on the tropical rainfall measuring mission satellite. part i: Methodology," *Journal of Applied Meteorology* **42**, pp. 240–265, 2003.
10. J. Townshend, C. Justice, D. Skole, J.-P. Malingreau, J. Cihlar, P. Teillet, F. Sadowski, , and S. Ruttenberg, "The 1-km avhrr global data set: needs of the international geosphere biosphere program," *International Journal for Remote Sensing* **15**, pp. 3319–3332, 1994.
11. A. Ipe, N. Clerbaux, C. Bertrand, D. S., and L. Gonzalez, "Pixel-scale composite toa clear-sky reflectances for meteosat-7 visible data," *Journal of Geophysical Research* **?**, p. accepted, 2003.
12. J. Schmetz and Q. Liu, "Outgoing longwave radiation and its diurnal variation at regional scales derived from meteosat," *Journal of Geophysical Research* **93**, pp. 11192–11204, September 1988.
13. N. Clerbaux, A. Ipe, C. Bertrand, D. S., B. Nicula, and L. Gonzalez, "Evidence of azimuthal anisotropy for the thermal infrared radiation leaving the earth's atmosphere," *International Journal for Remote Sensing* **24**, pp. 3005–3010, 2003.
14. L. Gonzalez, A. Hermans, S. Dewitte, A. Ipe, G. Sadowski, and N. Clerbaux, "Resolution enhancement of GERB data," in *Proc. of the 2000 EUMETSAT Meteorological Satellite Data User's Conference.*, pp. 619–625, (Bologna, Italy), May 29 – June 2 2000.
15. S. Dewitte, G. Sadowski, and L. Gonzalez, "L2 RMIB GERB products user guide," Tech. Rep. MSG-RMIB-GE-UG, RMIB, <http://gerb.oma.be>, 2002.